coatings

MDPI

Article

Molecular Dynamical Investigation of Lithium-Ion Adsorption on Multilayer Fullerene

Jinbin Lu [1], Jie Guan [1], Hao Chen [1,2], Minghua Li [2], Zhongwei Hua [3], Fuzhou Niu [1,2,*] and Yang Zhang [3,4,*]

[1] School of Mechanical Engineering, Suzhou University of Science and Technology, Suzhou 215009, China
[2] Jiangsu Juli Intelligent Machinery Co., Ltd., Suzhou 215009, China
[3] School of Science, Nanjing University of Science and Technology, Nanjing 210094, China
[4] Department of Architecture and Civil Engineering, City University of Hong Kong, Kowloon, Hong Kong, China
* Correspondence: fzniu@usts.edu.cn (F.N.); hfutzy@njust.edu.cn (Y.Z.)

Abstract: As the cathode of lithium-ion batteries, carbon material has been the focus of research. At present, diverse investigations have been carried out on the lithium convergence behavior in the carbon material family. As a new carbon material, multilayer fullerenes have been shown in various experimental studies to have a high discharge rate as an electrode, indicating that onion-like carbon has the potential to release energy quickly. Materials and mechanical scientists are increasingly interested in lithium-ion batteries. In this paper, the molecular dynamics (MD) method was used to simulate the absorption of lithium ions by multilayer fullerenes. A model of five layers of fullerenes was established to compare the lithium-ion absorption rates of multiple layers of fullerenes at different lithium-ion concentrations. The effects of the lithium-ion diffusion rate on the results were considered. In addition, the effects of the number of lithium ions, the velocity, and the layer number of multilayer fullerenes on the structural behavior and stress were investigated thoroughly when the multilayer fullerenes adsorbed lithium ions.

Keywords: molecular dynamics (MD) method; multilayer fullerene; lithium-ion battery; diffusion-induced stress

Citation: Lu, J.; Guan, J.; Chen, H.; Li, M.; Hua, Z.; Niu, F.; Zhang, Y. Molecular Dynamical Investigation of Lithium-Ion Adsorption on Multilayer Fullerene. *Coatings* **2022**, *12*, 1824. https://doi.org/10.3390/coatings12121824

Academic Editor: Alessandro Latini

Received: 27 October 2022
Accepted: 23 November 2022
Published: 25 November 2022

1. Introduction

Carbon materials have always been the focus of energy applications. The focus of attention has shifted from the continuous use of coal as the primary energy source to standard lithium-ion battery anode materials. In recent years, new types of carbon nanoforms with carbon nanotubes and graphene as the main directions have emerged. There is no doubt that this process has promoted research related to electrochemical energy storage and conversion, leading to the birth of a "new era of carbon" [1]. There are many different carbon nanoforms and allotropes in the carbon family. Among them, the multi-layer fullerene, which is also called onion-like carbon (OLC) or carbon nano onion (CNO), is the most interesting one. Multilayer fullerenes are approximately spherical nanoscale carbon particles composed of multiple closed fullerene-like carbon shells. They have a concentric layered structure similar to onions. In addition to being called CNO and OLC, multilayer fullerenes are also called superfullerenes or onion-like fullerenes. These names include various concentric shells ranging from nested fullerenes to small (<100 nm) polyhedral nanostructures, discovered by Iijima et al. [2]. In 1980, Ugarte et al. [3] synthesized and described multilayer fullerenes in amorphous carbon black. After only 20 years, Mordkovich [4] reported the first experimental observations of two-layer and three-layer multilayer fullerenes in 2000. Ostroumova et al. [5] conducted a reactive molecular dynamics study on the formation of onion-like carbon nanoparticles. The team of Dastjerdi et al. [6] conducted an in-depth study on the bending analysis of the fullerene structure. Gu et al. [7] studied the electrochemical properties of 5–10 nm onion-like carbon nanoparticles,

the presence and absence of functional groups on the surface of these nanoparticles, and non-diamond soot with similar particle morphology and mesoporous activated carbon. Wang et al. [8] used molecular mechanics calculations to generate geometrically optimized structures of large spherical fullerenes.

Multilayer fullerenes have a unique combination of high conductivity (compared to carbon black), large surface area and nanometer size (generally no more than 10 nm), and the possibility of large-scale synthesis and chemical modification [9]. From biomedical imaging [9] to electrochemical energy storage (EES) [10], lubrication and catalysis [11], and water treatment [12], this material has been advantageous. In EES applications, whether it is electrode materials for ultrafast charge/discharge devices [13], or conductive additives used to enhance the power-handling capability of activated carbon [14], multi-layer fullerenes have been widely used. Currently, there is more and more research on multilayer fullerenes for advanced electrochemical applications [15,16] due to the fast ion/electron transfer characteristics leading to the stable porous nanosphere structure formed by multilayer fullerenes with good electrochemical properties [17].

To deepen our understanding of the diffusion-induced stress in multi-layer fullerene during the lithium-ion diffusion process, the present work mainly studies the coupled effect of lithium intercalation behavior and multilayer fullerene structure behavior considering the influence of the velocity and concentration of lithium ions and the number of layers of multilayer fullerenes.

In this paper, MD was used to study the lithium insertion behavior in multilayer fullerenes. Molecular dynamics has a powerful ability to simulate the motion process of atoms, but it has not been reported on the motion evolution law and stress distribution of fullerene electrodes in the process of lithium-ion diffusion. Lithium ions contact and diffuse on the surface of multilayer fullerenes. Compared to macroscopic simulations, MD can help gain detailed insights into the microscopic mechanism of Li-ion intercalation into fullerene electrodes.

First, a model of five layers of fullerenes was established to compare the lithium-ion absorption rates of multiple layers of fullerenes at different lithium-ion concentrations. Then, we consider the effect of the lithium-ion diffusion rate on the results. Finally, we compared the effects of different layers on the stress changes of multilayer fullerenes. The results show that the concentration of lithium ions is positively correlated with the stress change of multilayer fullerenes. The higher the concentration is, the greater the stress fluctuation is. However, due to the limited amount of lithium ions adsorbed by multilayer fullerenes, increasing the concentration of lithium ions after exceeding the maximum adsorption concentration has little influence on the stress change. The velocity also directly affects the stress fluctuations produced by the multilayer fullerenes. The higher the velocity, the greater the stress fluctuation produced by multilayer fullerenes at the same concentration. In addition, the influence of the number of layers on the stress change is negatively correlated. The more layers, the less stress fluctuation.

2. Simulation Method

In this study, all the simulations are performed with the Large-scale Atomic/Molecular Massively Parallel Simulator (LAMMPS, Sandia National Laboratories, Albuquerque, NM, Sandia, USA) package [18], and atom visualization is done by the Open Visualization Tool (Ovito, OVITO Basic, Darmstadt, Germany) [19].

MD has been widely used to investigate the mechanical behavior of various nanostructures. For example, MD has been adopted to study the interaction between graphene [20–27], carbon nanotubes [28,29] and lithium ions, respectively. Furthermore, MD is also employed to examine the interaction between fullerene and potassium ion, which is called the inner membrane potassium ion fullerene ($K^+@C_{60}$) [30–32]. In addition, there are many studies on the interaction between spherical molecules, such as fullerenes using M [33–36]. Most of the above-mentioned papers adopted the adaptive intermolecular reactive empirical bond

order (AIREBO) [37] force field to study the mechanical properties of carbon systems. In this paper, AIREBO potential is also used to describe the interaction between carbon and carbon.

Apart from the bonding interaction that AIREBO describes, the nonbonding interaction, such as the van der Waals (vdW) interaction and Coulomb interaction, also needs to be considered. The Lennard-Jones (*LJ)* 12-6 potential is used to describe the vdW interaction of carbon–lithium and lithium–lithium pairs as

$$E_{LJ} = D_{ij}\left[\left(\frac{\sigma_{ij}}{r}\right)\left(\frac{\sigma_{ij}}{r}\right)^{12} - \left(\frac{\sigma_{ij}}{r}\right)\left(\frac{\sigma_{ij}}{r}\right)^{6}\right](r < r_c) E_{LJ} = D_{ij}\left[\left(\frac{\sigma_{ij}}{r}\right)\left(\frac{\sigma_{ij}}{r}\right)^{12} - \left(\frac{\sigma_{ij}}{r}\right)\left(\frac{\sigma_{ij}}{r}\right)^{6}\right](r < r_c)$$

where D_{ij} and σ_{ij} are the Lennard-Jones potential parameters and r_{ij} is the interatomic distance between the i th and j th atoms [38]. The potential energy parameters used in the present simulation are shown in Table 1.

Table 1. Potential energy parameters.

Parameter	Value
D_C [a]	0.1050
D_{Li} [a]	0.0250
σ_C [b]	3.8510
σ_{Li} [b]	2.4510

[a] D is in kcal/mol. [b] σ is in Å. In the calculation of D_{ij} and σ_{ij}, the arithmetic means [38] were used.

In the system, the Coulomb interaction affects C-Li, Li-Li, expressed as

$$E_{Coulomb} = \frac{Cq_iq_j}{r_{ij}}\ (r < r_c)$$

where q_i and q_j are the net atomic charges of i th and j th atoms, respectively.

The formula for the combination of carbon and lithium is

$$6C + Li^+ + e^- \rightleftharpoons Li^{\delta+}\ C_6{}^{\delta-}$$

δ_{Li} was fixed as 0.68 for the different stages in this study [38].

2.1. Simulation Process

In this paper, the single-layer fullerene model is combined, and the combined model is fully relaxed in Lammps to obtain the required multilayer fullerene molecular model, i.e., five-layer and three-layer multilayer fullerene, respectively. An Intel core i5 Duo 3.0-GHz processor running Windows 10 (Thinkpad X220, Lenovo, Beijing, China) is used for the simulations.

Firstly, as illustrated in Figure 1a, we add lithium ions along the Z-axis in the base model. For simplicity, a cylindrical boundary is set to limit the movement of lithium ions. To avoid interaction between lithium-ion atoms and multilayer fullerene atoms during the relaxation period, the distance between bottom lithium ions and the multilayer fullerene surface is not less than 1 nm. Then, the whole system is equilibrated for 15 ps using a canonical ensemble (NVT). The Nosé–Hoover thermostat is used to keep the temperature 300 K in the simulation. The time step is taken as 0.01 fs.

Secondly, lithium ions are distributed in a cylindrical space after equilibrium, and the model energy reaches the lowest state. Then, the lithium ions diffuse for 10 ps using NVT. In this stage, the time step is taken as 0.005 fs to capture a more detailed movement message. As the lithium ions move, they will collide and then be adsorbed by the multilayer fullerene. When the moving lithium ions are absorbed, the multilayer fullerene will move slightly along the negative direction of the Z-axis (as shown in Figure 1). In Figure 1, the lilac particles are lithium ions.

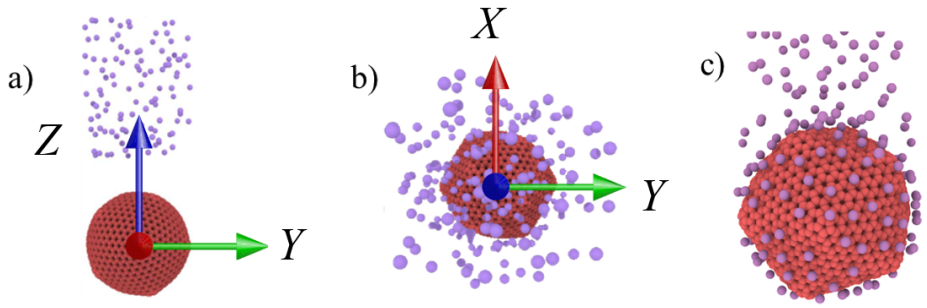

Figure 1. (**a**) Front view of the model. (**b**) Top view of the model. (**c**) Multilayer fullerenes adsorb moving lithium ions.

Due to the nature of the multilayer fullerenes, lithium ions enter the multilayer fullerenes with great difficulty. Only the adsorption of lithium ions on the surface of multilayer fullerenes is considered in this paper.

In the simulation process, lithium ions only adsorb on the surface of multilayer fullerenes, so the calculation of lithium-ion concentration only considers the outermost layer, C1500. The value of lithium-ion concentration in the simulation process is shown in Table 2. It can be seen that both the lithium-ion ratio and concentration are positively correlated with the number of the lithium ions in the whole system. The ratio is the ratio between the number of lithium ions and the outermost layer of the multilayer fullerene, C1500. The concentration causes the spatial distribution of lithium ions.

Table 2. The lithium-ion ratio corresponds to the lithium-ion concentration.

Number	Ratio	Concentration (atoms/nm^3)
50	0.033	0.46
100	0.067	0.92
150	0.1	1.38
200	0.133	1.85
250	0.167	2.31
300	0.2	2.77

In addition, considering the impact of lithium-ion velocity on the results, we set the comparison under different velocities, which are 10, 20, 30, and 40 (The unit is Å/ps).

In the whole simulation, we respectively compared the influence of different concentrations on the results when the velocity was 20 Å/ps and 40 Å/ps, and the influence of different velocities on the results when the ratio was 0.2.

2.2. Stress Calculation

Strictly speaking, stress is uncertain for a single atom and can only be calculated meaningfully for an influential group of atoms. Calculating the atomic stress of a single carbon atom only follows the concept of stress, which has completely different characteristics from macroscopic stress. At present, analysis of stress has been widely used in much MD research [39–43].

The atomic stress of each atom calculated by LAMMPS is the negative value of the pressure tensor of each atom, which is expressed as *Stress* × *Volume*. In the calculation process of Lammps, the atomic stress tensor of the atom α is given by the following formula, where a and b take the values x, y, and z to generate the components of the tensor:

$$S_{ab}^{\alpha} = -m^{\alpha} v_a^{\alpha} v_b^{\alpha} - W_{ab}.$$

The first term is a kinetic-energy contribution for atom α. The second term is the virial contribution due to intra- and intermolecular interactions. Most researchers adopt the following expression to calculate atomic stress,

$$\sigma_{ab}^{\alpha} = -\frac{1}{V_{\alpha}}\left(-m^{\alpha}v_{a}^{\alpha}v_{b}^{\alpha} - \sum_{\beta}F_{a}^{\alpha\beta}r_{b}^{\alpha\beta}{}_{ab}\right)$$

where V^{α} is the atomic volume of atom α, $F_{a}^{\alpha\beta}$ is the a-component of the force between atom α and atom β obtainable from the derivative of the potential, and r_{ab}^{b} represents the scalar components of the distance vector r_{ab}.

This means that in order to compute atomic stress σ_{ab}^{α}, S_{ab}^{α} must be divided by the volume of each atom. However, the volume of a single atom is difficult to calculate. Therefore, microscopic unit volume V (namely, equivalent unit) is adopted instead of the volume of a single atom to compute atomic stress, as depicted in Figure 2. The stress of a group of carbon atoms can be obtained as follows:

$$\sigma_{ab} = -\frac{1}{V}\sum_{\alpha}\left(-m^{\alpha}v_{a}^{\alpha}v_{b}^{\alpha} - \sum_{\beta}F_{a}^{\alpha\beta}r_{b}^{\alpha\beta}{}_{ab}\right).$$

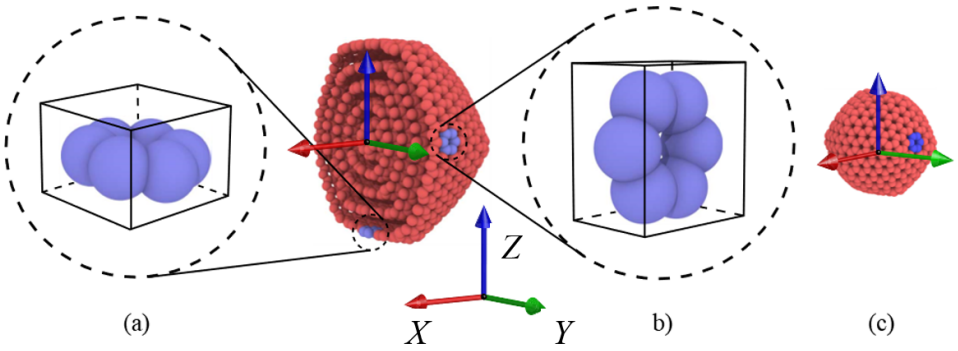

Figure 2. Two sets of carbon atoms are taken on the surface of five-layer multilayer fullerene (**a**) group 5L5Y (**b**) group 5L5(-Z). (**c**) A group of carbon atoms 5L3Y were taken from the surface of the three-layered fullerenes.

To reduce possible errors and be as objective as possible, we studied two sets of carbon atoms (blue atoms). One group is located at the fifth layer along the positive Y axis (located on the side of a multilayer fullerene), namely, group 5L5Y, as shown in Figure 3a,b. The other group is located at the fifth layer along the negative Z axis (on the underside of a multilayer fullerene), namely, group 5L5(-Z). To study the influence of the number of layers on the stress, a group of atoms, namely, group 3L3Y, was taken at the same position on the surface of the three-layer fullerene, as shown in Figure 2c, for comparison. After relaxation, the stress is extracted every 100 steps.

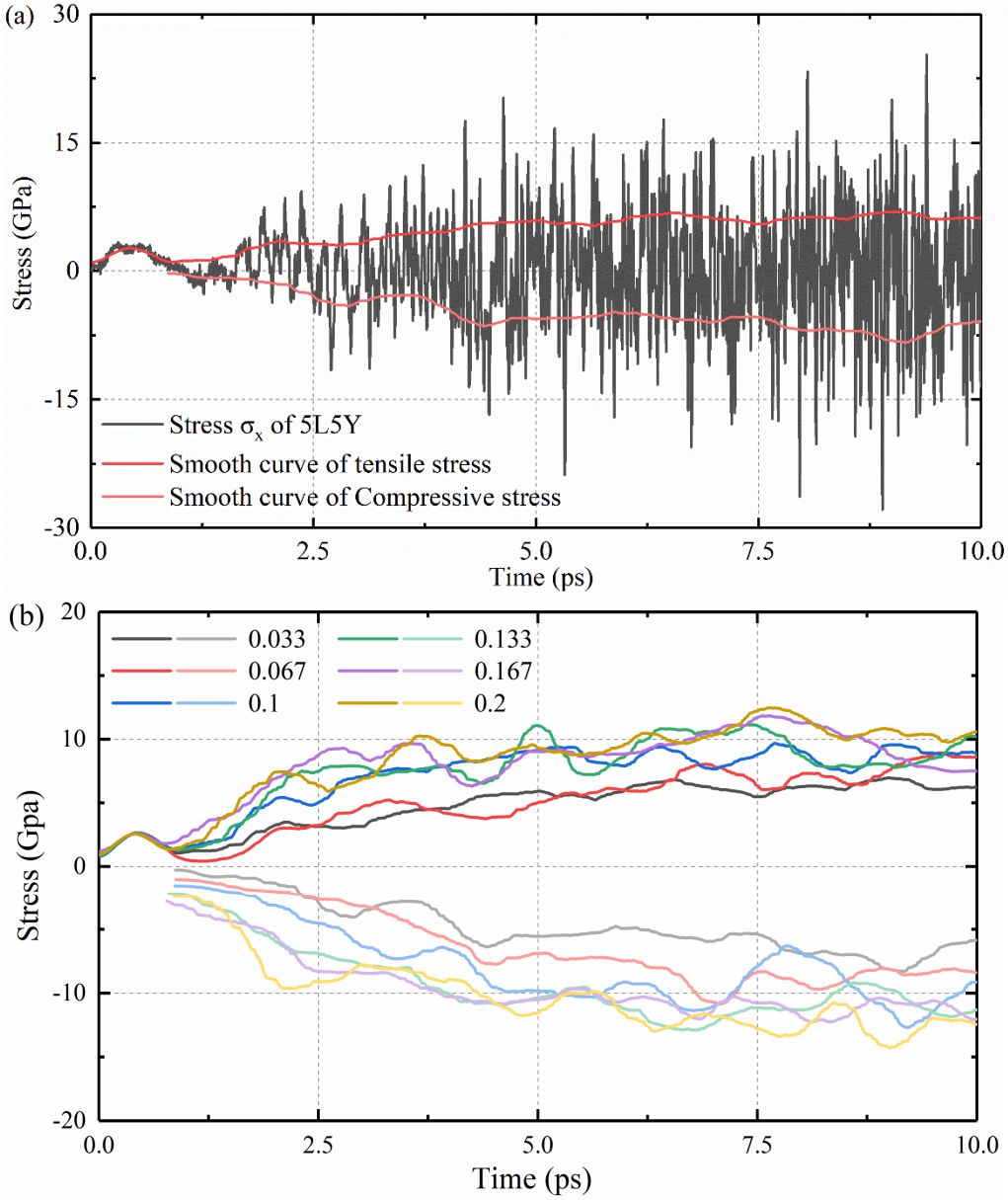

Figure 3. (**a**) The stress component σ_x generated by group 5L5Y was displayed before and after smoothing; (**b**) The stress component σ_x generated by group 5L5Y at different concentrations was compared after smoothing.

3. Results and Discussions

When the multilayer fullerene adsorbs lithium ions, the stress will change with the increase of lithium-ion concentration. Figure 3 shows the stress component σ_x generated by group 5L5Y when the ratio is 0.2 and the velocity is 20 Å/ps. It can be seen that the stress fluctuated greatly after the multilayer fullerene adsorbed lithium ions. Traditionally, negative stress means attraction, whereas positive stress means repulsion. For the convenience of display, we smooth the data of tensile stress and compressive stress respectively, as shown in the red and blue lines. When the velocity of the lithium ion is 20 Å/ps, the smooth curve of the stress component σ_x generated by group 5L5Y under different lithium-ion concentrations is compared. It can be seen that with the increase of lithium-ion concentration, the smooth stress curve gradually increases, but the degree of increase gradually decreases. The same situation is shown using the variance, as shown in Table 3, which shows the variance of the stress component data in the three directions of 5L5Y and

5L5(-Z) for two sets of the carbon atom. Except that the variance of σ_y of group 5L5Y and σ_z of group 5L5(-Z) is very small, the variance of other stress components increases with the increase of concentration. This indicates that the increase in concentration will gradually increase the fluctuations of the stress components of each group of carbon atoms, and the whole system becomes more and more active. However, when the concentration reaches a certain degree, the number of lithium ions that the system can absorb approach saturation, and the influence of the concentration on the stress change gradually decreases. When the speed is 40 Å/ps, the same results are shown in each group of data, as shown in Table 4. In addition, due to the fact that the multilayer surface of fullerenes in the set range is small, and because of the layers of the fullerenes' layered structure, the carbon atoms in the two groups will show the nature of the two-dimensional material. However, inevitably, due to deformation in the process of simulation of extrusion interaction with the other layers, the stress will fluctuate less. Although it is not apparent, it can still be seen that due to the increase of concentration, it also presents a slightly increasing trend.

Table 3. The variance of the stress components at the velocity is 20 Å/ps.

Concentration (atoms/nm^3)	Group 5L5Y			Group 5L5(-Z)		
	σ_x	σ_y	σ_z	σ_x	σ_y	σ_z
0.033	6.24715	1.66906	6.42387	6.36227	6.28345	0.72257
0.067	7.70491	3.90405	8.48047	8.00011	7.94726	0.88737
0.1	9.59082	3.173	9.7935	9.45388	9.92849	1.15529
0.133	10.77693	3.87023	10.47897	10.89653	11.02246	2.29164
0.167	11.07554	3.34023	11.52931	11.12232	11.36959	2.67114
0.2	11.77553	3.87955	11.87052	11.37549	12.07888	3.01447

Table 4. The variance of the stress components at the velocity is 40 Å/ps.

Concentration (atom/nm^3)	Group 5L5Y			Group 5L5(-Z)		
	σ_x	σ_y	σ_z	σ_x	σ_y	σ_z
0.033	7.76728	1.63038	8.43773	8.11088	7.8469	0.9264
0.067	9.82621	3.51548	9.987	10.20131	10.47156	2.31871
0.1	12.75335	3.67027	13.49606	12.81874	12.90796	3.47614
0.133	14.15314	4.42892	14.05658	13.77621	14.353	4.56613
0.167	14.7284	4.11106	15.18183	14.79008	15.66053	4.48393
0.2	14.47299	4.65719	14.29492	14.68558	14.63591	4.79911

When the lithium-ion ratio was 0.2, we compared the results of four groups with different velocities, as shown in Table 5. It can be seen that with the increase of velocity, the variance of each stress component gradually increases, which means that with the increase of velocity, the fluctuation of stress in all directions generated by groups five and six increases. Even at saturation, an increase in the velocity of the lithium ions makes the carbon atoms in the multilayer fullerenes more active.

Table 5. The variance of the stress components at the ratio is 0.2.

Velocity (Å/ps)	Group 5L5Y			Group 5L5(-Z)		
	σ_x	σ_y	σ_z	σ_x	σ_y	σ_z
10	9.61928	3.20742	10.29145	9.41925	9.61151	1.90242
20	11.78373	3.88003	11.87032	11.37543	12.07914	3.01467
30	13.44391	4.34859	14.09353	13.96878	14.06485	3.8023
40	14.47299	4.65719	14.29492	14.68558	14.63591	4.79911

In the layer-number contrast study, the lithium ion concentration and the velocity ratio were kept the same and the five fullerenes were distributed into three layers and five layers

to simulate the fullerenes group 5L5Y's and group 3L3Y's variance of stress. In Table 6, we can see that when layers increase, the stress fluctuation of the layers of fullerenes is reduced. This shows that in the same situation, the increase of the layers increases the stability of the system. After lithium ion adsorption, the surface activity of carbon atoms is reduced, and the results are confirmed by the Dastjerdi [6] et al. With the increase of radius, the elastic modulus of the fullerene decreases gradually, so the larger the number of layers, the smaller the stress amplitude of the outermost layer. As the number of layers of multilayer fullerenes increases, the stress of multilayer fullerenes are decreased. Since lithium ions cannot enter the interior of multilayer fullerenes, the volume of multilayer fullerenes will directly affect the product, thus reducing the battery capacity.

Table 6. The variance of stress generated by multilayer fullerene with different layers under the same concentration.

-	σ_x	σ_y	σ_z
Group 5L5Y	11.77553	3.87934	11.87005
Group 3L3Y	16.67001	5.09723	15.54763

4. Conclusions

The effects of the concentration and velocity of lithium ions and the number of layers of multilayer fullerenes on the surface stress during the adsorption of lithium ions by multilayer fullerenes were studied. In the process of absorbing lithium ions, stress fluctuations occur. As the concentration of lithium ions increases, the carbon atoms on the surface of the multilayer fullerenes become more active, resulting in a greater range of stress fluctuations, and then gradually decrease their activity after the concentration of lithium ions reach a critical point. When the saturation concentration is reached, the influence of the concentration will gradually decrease. At the same time, the higher the velocity, the more active the carbon atoms on the surface of the multilayer fullerenes and the greater the stress fluctuations. The increase of the number of layers will reduce the active degree of carbon atoms and reduce the amplitude of stress fluctuation. The performance of the electrode is comprehensively influenced by the number of layers and lithium-ion velocity. Therefore, the appropriate concentration and velocity of lithium ions and the radius of the multilayer fullerenes will better optimize the charging performance of the multilayer fullerenes electrode batteries. Studying the stress evolution law of lithium ions in the fullerene electrode particle group is an important research direction for future studies and has great practical significance.

Author Contributions: Conceptualization, J.G., Z.H. and M.L.; methodology, J.G., J.L., M.L. and Y.Z.; software, J.G., Z.H., H.C. and M.L.; validation, J.L., F.N. and Y.Z.; formal analysis, J.G., Z.H. and M.L.; investigation, J.G., J.L., M.L. and Y.Z.; resources, J.L., F.N. and Y.Z.; data curation, J.G.; writing—original draft preparation, J.G.; writing—review and editing, F.N. and Y.Z.; visualization, M.L. and H.C.; supervision, F.N. and Y.Z.; project administration, F.N. and Y.Z.; funding acquisition, F.N. and Y.Z. All authors have read and agreed to the published version of the manuscript.

Funding: This work was supported in part by the National Natural Science Foundation of China under Grant No. 12272182 and No. 11902159, in part by the Natural Science Foundation of Jiangsu Province under Grant No. BK20190941, in part by China Postdoctoral Science Foundation under Grant No. 2020M681517 and No. 2020M671383, in part by Postdoctoral Science Foundation of Jiangsu Province under Grant No. 2020Z063, in part by Jiangsu Province High-level Innovation and Entrepreneurship Talent Project, in part by Jiangsu Province Qinglan Project, and in part by Hong Kong Scholars Program under Grant No. XJ2019016.

Institutional Review Board Statement: Not applicable.

Informed Consent Statement: Not applicable.

Data Availability Statement: The raw/processed data required to reproduce these findings cannot be shared at this time as the data also forms part of an ongoing study.

Conflicts of Interest: The authors declare no conflict of interest.

References

1. Neto, C.; Antonio, H. The carbon new age. *Mater. Today* **2010**, *13*, 12–17. [CrossRef]
2. Iijima, S. Direct observation of the tetrahedral bonding in graphitized carbon black by high resolution electron microscopy. *J. Cryst. Growth* **1980**, *50*, 675–683. [CrossRef]
3. Ugarte, D. Curling and closure of graphitic networks under electron-beam irradiation. *Nature* **1992**, *359*, 707–709. [CrossRef]
4. Mordkovich, V.Z.; Umnov, A.G.; Inoshita, T. Nanostructure of laser pyrolysis carbon blacks: Observation of multiwall fullerenes. *Int. J. Inorg. Mater.* **2000**, *2*, 347–353. [CrossRef]
5. Ostroumova, G.; Orekhov, N.; Stegailov, V. Reactive molecular-dynamics study of onion-like carbon nanoparticle formation. *Diam. Relat. Mater.* **2019**, *94*, 14–20. [CrossRef]
6. Dastjerdi, S.; Akgöz, B. On the statics of fullerene structures. *Int. J. Eng. Sci.* **2019**, *142*, 125–144. [CrossRef]
7. Gu, W.; Peters, N.; Yushin, G. Functionalized onion-like carbon, detonation nanodiamond and mesoporous carbon as cathodes in Li-ion electrochemical energy storage devices. *Carbon* **2013**, *53*, 292–301. [CrossRef]
8. Wang, B.C.; Wang, H.W.; Chang, J.C.; Tso, H.C.; Chou, Y.M. More spherical large fullerenes and multi-layer fullerene cages. *J. Mol. Struct. THEOCHEM* **2001**, *540*, 171–176. [CrossRef]
9. Bartelmess, J.; Giordani, S. Carbon nano-onions (multi-layer fullerenes): Chemistry and applications. *Beilstein. J. Nanotechnol.* **2014**, *5*, 1980–1998. [CrossRef]
10. Portet, C.; Yushin, G.; Gogotsi, Y. Electrochemical performance of onion-like carbon, nanodiamonds, carbon black and multiwalled nanotubes in electrical double layer capacitors. *Carbon* **2007**, *45*, 2511–2518. [CrossRef]
11. Crestani, M.G.; Puente-Lee, I.; Rendón-Vazquez, L.; Santiago, P.; del Rio, F.; Morales-Morales, D.; García, J.J. The catalytic reduction of carbon dioxide to carbon onion particles by platinum catalysts. *Carbon* **2005**, *43*, 2621–2624. [CrossRef]
12. Porada, S.; Borchardt, L.; Oschatz, M.; Bryjak, M.; Atchison, J.S.; Keesman, K.J.; Kaskel, S.; Biesheuvel, P.M.; Presser, V. Direct prediction of the desalination performance of porous carbon electrodes for capacitive deionization. *Energy Environ. Sci.* **2013**, *6*, 3700. [CrossRef]
13. Pech, D.; Brunet, M.; Durou, H.; Huang, P.; Mochalin, V.; Gogotsi, Y.; Taberna, P.-L.; Simon, P. Ultrahigh-power micrometre-sized supercapacitors based on onion-like carbon. *Nat. Nanotechnol.* **2010**, *5*, 651–654. [CrossRef]
14. Jäckel, N.; Weingarth, D.; Zeiger, M.; Aslan, M.; Grobelsek, I.; Presser, V. Comparison of onion-like carbon and carbon blacks as conductive additives for carbon supercapacitors in organic electrolytes. *J. Power Sources* **2014**, *272*, 1122–1133. [CrossRef]
15. McDonough, J.K.; Gogotsi, Y. Onion-like carbon: Synthesis and electrochemical applications. *Interface Mag.* **2013**, *22*, 61–66. [CrossRef]
16. Plonska-Brzezinska, M.E.; Echegoyen, L. Carbon nano-onions for supercapacitor electrodes: Recent developments and applications. *J. Mater. Chem. A* **2013**, *1*, 13703. [CrossRef]
17. Tang, W.; Wu, J.; Wang, X.; Xia, X.; Tu, J. Integrated carbon nanospheres arrays as anode materials for boosted sodium ion storage. *Green Energy Environ.* **2018**, *3*, 50–55. [CrossRef]
18. Plimpton, S. Fast parallel algorithms for short-range molecular dynamics. *J. Comput. Phys.* **1995**, *117*, 1–19. [CrossRef]
19. Stukowski, A. Visualization and analysis of atomistic simulation data with OVITO–the Open visualization tool. *Model. Simul. Mater. Sci. Eng.* **2009**, *18*, 015012. [CrossRef]
20. Ganesh, P.; Kim, J.; Park, C.; Yoon, M.; Reboredo, F.A.; Kent, P.R.C. Binding and diffusion of lithium in graphite: Quantum monte carlo benchmarks and validation of van der Waals density functional methods. *J. Chem. Theory Comput.* **2014**, *10*, 5318–5323. [CrossRef]
21. Kühne, M.; Börrnert, F.; Fecher, S.; Ghorbani-Asl, M.; Biskupek, J.; Samuelis, D.; Krasheninnikov, A.; Kaiser, U.; Smet, J.H. Reversible superdense ordering of lithium between two graphene sheets. *Nature* **2018**, *564*, 234–239. [CrossRef] [PubMed]
22. McNutt, N.W.; Rios, O.; Maroulas, V.; Keffer, D.J. Interfacial Li-ion localization in hierarchical carbon anodes. *Carbon* **2017**, *111*, 828–834. [CrossRef]
23. Okamoto, H. The C-Li (Carbon-Lithium) system. *Bull. Alloy Phase Diagr.* **1989**, *10*, 69–72. [CrossRef]
24. Shi, H.; Barker, J.; Saïdi, M.Y.; Koksbang, R.; Morris, L. Graphite structure and lithium intercalation. *J. Power Sources* **1997**, *68*, 291–295. [CrossRef]
25. Shimizu, A.; Tachikawa, H. The dynamics on migrations of Li^+ ion and Li atom at 700 K around the circumference of graphite cluster model: A direct molecular dynamics study. *Chem. Phys. Lett.* **2001**, *339*, 110–116. [CrossRef]
26. Kganyago, K.R.; Ngoepe, P.E. Structural and electronic properties of lithium intercalated graphite. *Phys. Rev. B* **2003**, *68*, 205111. [CrossRef]
27. Zhang, R. Growth mechanism of Ni-graphene composite coating on mild steel: A combined experimental and molecular dynamics study. *Int. J. Electrochem. Sci.* **2022**, *17*, 220939. [CrossRef]
28. Chakraborti, N.; Das, S.; Jayakanth, R.; Pekoz, R.; Erkoç, Ş. Genetic algorithms applied to Li^+ ions contained in carbon nanotubes: An investigation using particle swarm optimization and differential evolution along with molecular dynamics. *Mater. Manuf. Processes* **2007**, *22*, 562–569. [CrossRef]
29. Ailenei, A.-E.; Beu, T.A. Ion transport through gated carbon nanotubes: Molecular dynamics simulations using polarizable water. *J. Mol. Struct.* **2021**, *1245*, 131022. [CrossRef]

30. Kang, J.W.; Hwang, H.J. A Bucky shuttle three-terminal switching device: Classical molecular dynamics study. *Phys. E Low-Dimens. Syst. Nanostructures* **2004**, *23*, 36–44. [CrossRef]
31. Kang, J.W.; Hwang, H.J. Model schematics of a nanoelectronic device based on multi-endo-fullerenes electromigration. *Phys. E Low-Dimens. Syst. Nanostructures* **2005**, *27*, 245–252. [CrossRef]
32. Piątek, A.; Dawid, A.; Gburski, Z. The properties of endohedral potassium ion fullerene cluster: MD simulation. *J. Mol. Struct.* **2008**, *887*, 144–147. [CrossRef]
33. Chen, L.; Wang, X.; Kumar, S. Thermal transport in fullerene derivatives using molecular dynamics simulations. *Sci. Rep.* **2015**, *5*, 12763. [CrossRef]
34. Hu, D.; Hu, J.; Jiang, H.; Xu, J. A highly effective energy mitigation system combining carbon nanotube and buckyballs. *Eur. Phys. J. Spec. Top.* **2018**, *227*, 155–166. [CrossRef]
35. Silveira, J.F.; Pagnussati, R.A.; Kleinpaul, J.; Paupitz, R.; Muniz, A.R. Nanoporous carbon superstructures based on covalent bonding of porous fullerenes. *Carbon* **2018**, *130*, 424–432. [CrossRef]
36. Sun, W.; Zeng, Q.; Yu, A. Interaction forces between carbon nanospheres: A molecular dynamics simulation study. *Chem. Eng. Sci.* **2015**, *121*, 23–31. [CrossRef]
37. Stuart, S.J.; Tutein, A.B.; Harrison, J.A. A reactive potential for hydrocarbons with intermolecular interactions. *J. Chem. Phys.* **2000**, *112*, 6472–6486. [CrossRef]
38. Song, M.K.; Hong, S.D.; No, K.T. The structure of lithium intercalated graphite using an effective atomic charge of lithium. *J. Electrochem. Soc.* **2001**, *148*, A1159. [CrossRef]
39. Frankland, S. The stress–strain behavior of polymer–nanotube composites from molecular dynamics simulation. *Compos. Sci. Technol.* **2003**, *63*, 1655–1661. [CrossRef]
40. Girifalco, L.A.; Hodak, M.; Lee, R.S. Carbon nanotubes, buckyballs, ropes, and a universal graphitic potential. *Phys. Rev. B* **2000**, *62*, 13104–13110. [CrossRef]
41. Li, X.; Song, W.; Smedskjaer, M.M.; Mauro, J.C.; Bauchy, M. Quantifying the internal stress in over-constrained glasses by molecular dynamics simulations. *J. Non-Cryst. Solids X* **2019**, *1*, 100013. [CrossRef]
42. Liu, B.; Qiu, X. How to compute the atomic stress objectively? *J. Comput. Theor. Nanosci.* **2009**, *6*, 1081–1089. [CrossRef]
43. Yang, J.; Komvopoulos, K. A stress analysis method for molecular dynamics systems. *Int. J. Solids Struct.* **2020**, *193–194*, 98–105. [CrossRef]